

Tensor-Based Channel Estimation and Data-Aided Tracking in IRS-Assisted MIMO Systems

Kenneth B. A. Benício, André L. F. de Almeida, *Senior Member, IEEE*, Bruno Sokal, Fazal-E-Asim, *Senior Member, IEEE*, Behrooz Makki, *Senior Member, IEEE*, and Gábor Fodor, *Senior Member, IEEE*

Abstract—This letter proposes a model for symbol detection in the uplink of intelligent reflecting surface (IRS)-assisted networks in the presence of channel aging. During the first stage, we model the received pilot signal as a tensor, which serves as a basis for both estimating the channel and configuring the IRS. In the second stage, the proposed tensor approach tracks the aging process to detect and estimate the transmitted data symbols. Our evaluations show that our proposed channel and symbol estimation schemes improve the performance of IRS-assisted systems in terms of the achieved bit error rate and mean squared error of the received data, compared to state of the art schemes.

Index Terms—channel aging, channel estimation, intelligent reflecting surfaces, tensor-based algorithm

I. INTRODUCTION

Over the last few years, IRS has been considered as one of the possible technologies to be deployed in beyond fifth generation (B5G) wireless networks due to their potential to improve system capacity [1]–[4]. An IRS is a 2D panel composed of many passive reflecting elements whose phase shifts are adjusted to maximize the signal-to-noise ratio (SNR) at the intended receiver [5]. Hence, channel estimation must be performed at the end nodes of the network and the receiver should estimate the involved channels from received pilots reflected by the IRS according to a training protocol. Several works have addressed this problem, e.g., [6]–[8]. As pointed out in [8], channel estimation methods can be divided into unstructured and structured methods, where the latter category exploits the parametric (geometric) modeling of the cascaded channel, which is the focus of the present work.

The authors in [6] use a tensor approach to perform supervised channel estimation. Then, [7] proposes a tensor-based receiver formulated as a semi-blind problem that jointly estimates the involved channels and transmitted data. However, these two works assume (quasi)-static channels and do not consider the aging problem, which is likely to be present due to user mobility. Finally, it is worth noting that the impact of channel aging in multiple input multiple output (MIMO) and IRS-assisted systems has been studied in [9]–[12] while the geometrical structure of the channel has not been exploited.

In this letter, we propose a signal modeling that exploits the geometric channel structure of the IRS-assisted MIMO

network to estimate the spatial signatures of the network. The time-varying fading coefficients are modeled by means of an auto-regressive (AR) model with each channel changing independently at different time scales. Then, we formulate a two-stage tensor-based framework for parameter estimation and data-aided tracking. In the first stage, referred to as PARAFAC-Khatri-Rao-Kronecker factorization (PARKRON), the estimation of channel steering vectors (static parameters) is carried out by means of a constrained tensor-based solution. Then, in the second stage, referred to as Tucker-based tracking (TBT), we perform data-aided tracking of channel fading coefficients and symbol detection. Simulation results show that our proposed method accurately tracks the cascaded channel while outperforming competing methods in terms of normalized mean squared error (NMSE).

Notation: Scalars, vectors, matrices, and tensors are represented by $a, \mathbf{a}, \mathbf{A}$, and \mathcal{A} . Also, \mathbf{A}^* , \mathbf{A}^T , \mathbf{A}^H , and \mathbf{A}^\dagger stand for the conjugate, transpose, Hermitian, and pseudo-inverse, of a matrix \mathbf{A} . The j th column of $\mathbf{A} \in \mathbb{C}^{I \times J}$ is denoted by $\mathbf{a}_j \in \mathbb{C}^{I \times 1}$. The operator $\text{vec}(\cdot)$ transforms a matrix into a vector by stacking its columns, e.g., $\text{vec}(\mathbf{A}) = \mathbf{a} \in \mathbb{C}^{I \times J \times 1}$, while the $\text{unvec}(\cdot)_{I \times J}$ operator undo the operation. The operator $\text{D}(\cdot)$ converts a vector into a diagonal matrix, $\text{D}_j(\mathbf{B})$ forms a diagonal matrix $R \times R$ out of the j th row of $\mathbf{B} \in \mathbb{C}^{J \times R}$. Also, \mathbf{I}_N denotes an identity matrix of size $N \times N$. The symbols \otimes and \diamond indicate the Kronecker and Khatri-Rao products.

II. SYSTEM MODEL

We consider an uplink IRS-assisted MIMO scenario with a base station (BS) equipped with M receiver antennas, which receives a signal from a user equipment (UE) equipped with Q transmit antennas *via* a passive IRS with N reflecting elements. The transmission protocol is structured as I frames each one containing $K + 1$ blocks. The first block has length T_0 symbol periods, while the remaining K blocks have length $(T_p + T_d)$, as shown in Fig 1. The first block ($k = 1$) of each frame is dedicated to pilot-aided parameter estimation, and the received signal is given by

$$\mathbf{y}_{i,1,t} = \mathbf{G}_i \text{D}(\mathbf{s}_t) \mathbf{H}_{i,1} \mathbf{z}_{i,t} + \mathbf{v}_{i,1,t} \in \mathbb{C}^{M \times 1}, \quad (1)$$

where $\mathbf{z}_{i,t}$ is the pilot sequence and $\mathbf{v}_{i,1,t}$ is the additive white Gaussian noise (AWGN) vector with $t \in \{1, \dots, T_0\}$. For the remaining K blocks, the received signal can be written as

$$\mathbf{Y}_{i,k} = \mathbf{G}_i \text{D}(\mathbf{s}_{\text{opt}}) \mathbf{H}_{i,k} \mathbf{X}_i + \mathbf{V}_{i,k} \in \mathbb{C}^{M \times (T_p + T_d)}, \quad (2)$$

This work was supported by the Ericsson Research, Sweden, and Ericsson Innovation Center, Brazil, under UFC.51 Technical Cooperation Contract Ericsson/UFC. This study was financed in part by CAPES/Brazil - Finance Code 001, and CAPES/PRINT Proc. 88887.311965/2018-00. André L. F. de Almeida thanks CNPq for its financial support under grant 312491/2020-4. G. Fodor was partially supported by the Digital Futures project PERCY.

where $\mathbf{Y}_{i,k} = [\mathbf{Y}_{i,k}^{(p)} | \mathbf{Y}_{i,k}^{(d)}] \in \mathbb{C}^{M \times (T_p + T_d)}$ and $\mathbf{X}_i = [\mathbf{X}_i^{(p)} | \mathbf{X}_i^{(d)}] \in \mathbb{C}^{Q \times (T_p + T_d)}$ are the received and the transmitted signals containing both pilots and data, spanning $T = T_p + T_d$ symbol periods each, where the pilot signals $\mathbf{Y}_{i,k}^{(p)} = [\mathbf{Y}_{i,k,1}^{(p)}, \dots, \mathbf{Y}_{i,k,T_p}^{(p)}] \in \mathbb{C}^{M \times T_p}$ and $\mathbf{X}_i^{(p)} = [\mathbf{X}_{i,1}^{(p)}, \dots, \mathbf{X}_{i,T_p}^{(p)}] \in \mathbb{C}^{Q \times T_p}$ have a duration of T_p symbols and the data signals $\mathbf{Y}_{i,k}^{(d)} = [\mathbf{Y}_{i,k,1}^{(d)}, \dots, \mathbf{Y}_{i,k,T_d}^{(d)}] \in \mathbb{C}^{M \times T_d}$ and $\mathbf{X}_i^{(d)} = [\mathbf{X}_{i,1}^{(d)}, \dots, \mathbf{X}_{i,T_d}^{(d)}] \in \mathbb{C}^{M \times T_d}$ have a duration of T_d symbols, respectively, in accordance to Fig. 1. At the time instant t , $\mathbf{D}(s_t)$ is the IRS phase-shift matrix, $\mathbf{D}(s_{\text{opt}})$ the IRS optimal phase-shift matrix obtained at the first block ($k = 1$), $\mathbf{X}_i^{(p)}$ is the pilot sequence, $\mathbf{X}_i^{(d)}$ is the data sequence.

We assume that the IRS-UE link changes faster due to mobility while the BS-IRS link changes more slowly due to possible changes in interference. Specifically, the IRS-UE channel $\mathbf{H}_{i,k}$ changes between blocks within a given frame, while the BS-IRS channel \mathbf{G}_i changes at a larger time scale, remaining constant during a frame of $K + 1$ blocks while varying across the I frames. Assuming a mmWave scenario, we adopt a multipath channel model [13] for the involved channels. We can express these channel matrices as follows

$$\mathbf{G}_i = \mathbf{A}_{\text{rx}} \mathbf{D}(\boldsymbol{\alpha}_i) \mathbf{B}_{\text{tx}}^H \in \mathbb{C}^{M \times N}, \quad (3)$$

$$\mathbf{H}_{i,k} = \mathbf{B}_{\text{rx}} \mathbf{D}(\boldsymbol{\beta}_{i,k}) \mathbf{A}_{\text{tx}}^H \in \mathbb{C}^{N \times Q}, \quad (4)$$

where \mathbf{A}_{rx} and \mathbf{B}_{rx} are the steering matrices defined as

$$\mathbf{A}_{\text{rx}} = [\mathbf{a}_{\text{rx}}(\mu_{\text{bs}}^{(1)}), \dots, \mathbf{a}_{\text{rx}}(\mu_{\text{bs}}^{(L_1)})] \in \mathbb{C}^{M \times L_1},$$

$$\mathbf{B}_{\text{rx}} = [\mathbf{b}_{\text{rx}}^{(\text{irs})}(\mu_{\text{irsA}}^{(1)}, \psi_{\text{irsA}}^{(1)}), \dots, \mathbf{b}_{\text{rx}}^{(\text{irs})}(\mu_{\text{irsA}}^{(L_2)}, \psi_{\text{irsA}}^{(L_2)})] \in \mathbb{C}^{N \times L_2},$$

with \mathbf{B}_{tx} and \mathbf{A}_{tx} being defined similarly. The l th BS steering vector $\mathbf{a}(\mu_{\text{bs}}^{(l)})$ is associated with the spatial frequency $\mu_{\text{bs}}^{(l)} = \pi \cos(\phi_{\text{bs}}^{(l)})$, with $\phi_{\text{bs}}^{(l)}$ being the angle of arrival (AoA), which can be further written as

$$\mathbf{a}_{\text{rx}}(\mu_{\text{bs}}^{(l)}) = [1, \dots, e^{-j\pi(M-1)\mu_{\text{bs}}^{(l)}}]^T \in \mathbb{C}^{M \times 1}. \quad (5)$$

Similarly, the p th one-dimensional steering vector for the UE is $\mathbf{c}(\mu_{\text{ue}}^{(p)})$ having spatial frequency, which is defined as $\mu_{\text{ue}}^{(p)} = \pi \cos(\phi_{\text{ue}}^{(p)})$, with $\phi_{\text{ue}}^{(p)}$ being the angle of departure (AoD), and can be written in terms of spatial frequency as

$$\mathbf{a}_{\text{tx}}(\mu_{\text{ue}}^{(p)}) = [1, \dots, e^{-j\pi(Q-1)\mu_{\text{ue}}^{(p)}}]^T \in \mathbb{C}^{Q \times 1}. \quad (6)$$

At the IRS, $\mathbf{b}_{\text{rx}}^{(\text{irs})}(\mu_{\text{irsA}}^{(l_2)}, \psi_{\text{irsA}}^{(l_2)})$ is the 2D steering vector with spatial frequencies $\mu_{\text{irsA}}^{(l_2)} = \pi \cos(\phi_{\text{irsA}}^{(l_2)}) \sin(\theta_{\text{irsA}}^{(l_2)})$ and $\psi_{\text{irsA}}^{(l_2)} = \pi \cos(\phi_{\text{irsA}}^{(l_2)})$, where $\phi_{\text{irsA}}^{(l_2)}$ and $\theta_{\text{irsA}}^{(l_2)}$ are the azimuth AoA and the elevation AoA, respectively. This can be further written as the Kronecker product between two steering vectors as

$$\mathbf{b}_{\text{rx}}^{(\text{irs})}(\mu_{\text{irsA}}^{(l_2)}, \psi_{\text{irsA}}^{(l_2)}) = \mathbf{b}_{\text{rx}}^{(\text{irs})}(\mu_{\text{irsA}}^{(l_2)}) \otimes \mathbf{b}_{\text{rx}}^{(\text{irs})}(\psi_{\text{irsA}}^{(l_2)}) \in \mathbb{C}^{N \times 1}. \quad (7)$$

The IRS transmission steering vector, $\mathbf{b}_{\text{tx}}^{(\text{irs})H}(\mu_{\text{irsD}}^{(l_1)}, \psi_{\text{irsD}}^{(l_1)})$, is defined similarly. The IRS phase-shift vector is defined as $\mathbf{s}_t = [e^{j\theta_{1,t}}, \dots, e^{j\theta_{N,t}}]^T \in \mathbb{C}^{N \times 1}$, where $\theta_{n,t}$ is the phase-shift of the n th IRS element at the t th time slot. Moreover, $\boldsymbol{\alpha}_i = [\alpha_i^{(1)}, \dots, \alpha_i^{(L_1)}]^T \in \mathbb{C}^{L_1 \times 1}$ and $\boldsymbol{\beta}_{i,k} = [\beta_{i,k}^{(1)}, \dots, \beta_{i,k}^{(L_2)}]^T \in$

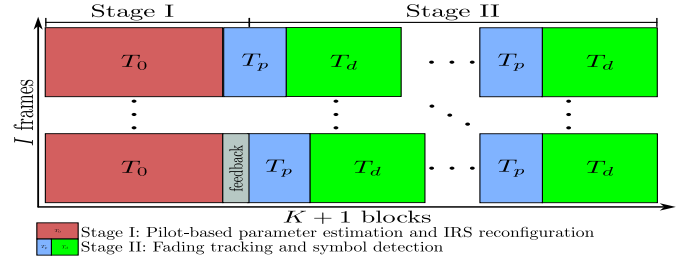


Fig. 1: Time-domain transmission protocol.

$\mathbb{C}^{L_2 \times 1}$ collect the path loss and fading components of the BS-IRS and IRS-UE links, respectively.

The aging effects are modeled by assuming that $\boldsymbol{\alpha}_i \in \mathbb{C}^{L_1 \times 1}$ and $\boldsymbol{\beta}_{i,k} \in \mathbb{C}^{L_2 \times 1}$ vary according to first-order AR processes defined as [9]

$$\boldsymbol{\alpha}_i = \delta \boldsymbol{\alpha}_{i-1} + \boldsymbol{\zeta}_i, \quad i = 1, \dots, I, \quad (8)$$

$$\boldsymbol{\beta}_{i,k} = \begin{cases} \lambda \boldsymbol{\beta}_{i-1,K} + \boldsymbol{\xi}_{i,k}, & k = 1, \\ \lambda \boldsymbol{\beta}_{i,k-1} + \boldsymbol{\xi}_{i,k}, & k = 2, \dots, K, \end{cases} \quad (9)$$

where $\boldsymbol{\zeta}_i \sim \mathcal{CN}(\mathbf{0}, (1 - \delta^2) \mathbf{I}_{L_1}) \in \mathbb{C}^{L_1 \times 1}$ and $\boldsymbol{\xi}_{i,k} \sim \mathcal{CN}(\mathbf{0}, (1 - \lambda^2) \mathbf{I}_{L_2}) \in \mathbb{C}^{L_2 \times 1}$ are the AR process noise term for the BS-IRS and IRS-UE links with δ and λ being their correlation coefficients [10], respectively.

III. PILOT-BASED PARAMETER ESTIMATION

In this section, we formulate the parameter estimation problem and describe the IRS phase-shift configuration approach shown in Algorithm 1 (PARKRON). Here, we estimate the channel parameters, i.e., the array steering matrices and the complex channel gains of the first block ($k = 1$) from all frames.

A. Tensor-Based Parameter Estimation

In this section, we formulate a tensor-based approach to estimate the channel parameters. Using $\text{vec}(\mathbf{ABC}) = (\mathbf{C}^T \otimes \mathbf{A}) \text{vec}(\mathbf{B})$ and $\text{vec}(\mathbf{AD}(\mathbf{b})\mathbf{C}) = (\mathbf{C}^T \diamond \mathbf{A}) \mathbf{b}$ in (1), yields

$$\mathbf{y}_{i,1,t} = \text{vec}(\mathbf{I}_M \mathbf{G}_i \mathbf{D}(s_t) \mathbf{H}_{i,1} \mathbf{z}_{i,t}) + \mathbf{v}_{i,1,t} \in \mathbb{C}^{M \times 1},$$

$$= (\mathbf{s}_t^T \otimes \mathbf{z}_{i,t}^T \otimes \mathbf{I}_M) \text{vec}(\mathbf{H}_{i,1}^T \diamond \mathbf{G}_i) + \mathbf{v}_{i,1,t}.$$

Collecting the signals during the T_0 symbol periods yields

$$\mathbf{y}_{i,1} = [\mathbf{y}_{i,1,1}^T, \dots, \mathbf{y}_{i,1,T_0}^T]^T,$$

$$= [(\mathbf{S} \diamond \mathbf{Z}_i)^T \otimes \mathbf{I}_M] \text{vec}(\mathbf{H}_{i,1}^T \diamond \mathbf{G}_i) + \mathbf{v}_{i,1} \in \mathbb{C}^{MT_0 \times 1},$$

$$= \boldsymbol{\Omega}_i \mathbf{u} + \mathbf{v}_{i,1} \in \mathbb{C}^{MT_0 \times 1}, \quad (10)$$

where $\mathbf{S} = [\mathbf{s}_1, \dots, \mathbf{s}_{T_0}] \in \mathbb{C}^{N \times T_0}$, $\mathbf{Z}_i = [\mathbf{z}_{i,1}, \dots, \mathbf{z}_{i,T_0}] \in \mathbb{C}^{Q \times T_0}$ are matrices collecting the IRS phase-shifts and pilots, $\boldsymbol{\Omega}_i = (\mathbf{S} \diamond \mathbf{Z}_i)^T \otimes \mathbf{I}_M \in \mathbb{C}^{MT_0 \times MQN}$, $\mathbf{u} = \text{vec}(\mathbf{H}_{i,1}^T \diamond \mathbf{G}_i) \in \mathbb{C}^{MQN \times 1}$, and $\mathbf{v}_{i,1} = [\mathbf{v}_{i,1,1}^T, \dots, \mathbf{v}_{i,1,T_0}^T]^T \in \mathbb{C}^{MT_0 \times 1}$ is the AWGN noise term. From (10), we obtain the following least squares (LS) problem

$$\hat{\mathbf{u}}_i = \arg \min_{\mathbf{u}_i} \|\mathbf{y}_{i,1} - \boldsymbol{\Omega}_i \mathbf{u}_i\|_2^2, \quad (11)$$

where the solution requires $T_0 \geq QN$ and is given by

$$\hat{\mathbf{u}}_i = \boldsymbol{\Omega}_i^\dagger \mathbf{y}_{i,1} \in \mathbb{C}^{MQN \times 1}. \quad (12)$$

Let us define $\mathbf{R}_i = \text{unvec}_{MQ \times N}(\hat{\mathbf{u}}_i) \approx \mathbf{H}_{i,1}^T \diamond \mathbf{G}_i \in \mathbb{C}^{MQ \times N}$. Using (3) and (4), while applying property $(\mathbf{A}\mathbf{C}) \diamond (\mathbf{B}\mathbf{D}) = (\mathbf{A} \otimes \mathbf{B})(\mathbf{C} \diamond \mathbf{D})$, we have

$$\begin{aligned} \mathbf{R}_i &\approx [\mathbf{A}_{\text{rx}}^* \mathbf{D}(\beta_i) \mathbf{B}_{\text{rx}}^T] \diamond [\mathbf{A}_{\text{rx}} \mathbf{D}(\alpha_i) \mathbf{B}_{\text{rx}}^H], \\ &\approx (\mathbf{A}_{\text{rx}}^* \otimes \mathbf{A}_{\text{rx}}) [\mathbf{D}(\beta_i) \otimes \mathbf{D}(\alpha_i)] (\mathbf{B}_{\text{rx}}^T \diamond \mathbf{B}_{\text{rx}}^H). \end{aligned} \quad (13)$$

Defining $\mathbf{F} = [\mathbf{f}_1, \dots, \mathbf{f}_I]^T \in \mathbb{C}^{I \times L_1 L_2}$ with $\mathbf{f}_i = \beta_i \otimes \alpha_i \in \mathbb{C}^{L_1 L_2 \times 1}$, (13) can be expressed as

$$\mathbf{R}_i \approx (\mathbf{A}_{\text{rx}}^* \otimes \mathbf{A}_{\text{rx}}) \mathbf{D}_i(\mathbf{F}) \mathbf{P}_B^T \in \mathbb{C}^{MQ \times N}, \quad (14)$$

where $\mathbf{P}_B = (\mathbf{B}_{\text{rx}}^T \diamond \mathbf{B}_{\text{rx}}^H) \in \mathbb{C}^{N \times L_1 L_2}$ combines the IRS transmit and receive steering matrices. The collection of matrices $\{\mathbf{R}_1, \dots, \mathbf{R}_I\}$, in (14) over all frames $i \in \{1, \dots, I\}$ can be arranged as a fourth-way tensor $\mathcal{R} \in \mathbb{C}^{M \times Q \times N \times I}$, which can be expanded in terms of n -mode products as

$$\mathcal{R} \approx \mathcal{I}_{4, L_1 L_2} \times_1 (\mathbf{A}_{\text{rx}} \boldsymbol{\Psi}) \times_2 (\mathbf{A}_{\text{rx}}^* \boldsymbol{\Phi}) \times_3 \mathbf{P}_B \times_4 \mathbf{F}, \quad (15)$$

where $\boldsymbol{\Psi} = \mathbf{1}_{L_1}^T \otimes \mathbf{I}_{L_2} \in \mathbb{R}^{L_2 \times L_1 L_2}$ and $\boldsymbol{\Phi} = \mathbf{I}_{L_1} \otimes \mathbf{1}_{L_2}^T \in \mathbb{R}^{L_1 \times L_1 L_2}$ are constraints matrices. This tensor structure follows a constrained PARAFAC decomposition, which can also be interpreted as a constrained factor decomposition [14] or parallel profiles with linear dependencies decomposition [15]. Assuming that the BS and the IRS have fixed and known locations, it is reasonable to consider that the angular information between the IRS and the BS is known, i.e., we assume the knowledge of the steering matrix \mathbf{A}_{rx} . Consequently, the estimation of \mathbf{A}_{tx} , \mathbf{P}_B and \mathbf{F} consists of solving the following problem

$$\left\{ \hat{\mathbf{A}}_{\text{tx}}, \hat{\mathbf{P}}_B, \hat{\mathbf{F}} \right\} = \arg \min_{\mathbf{A}_{\text{tx}}, \mathbf{P}_B, \mathbf{F}} \left\| \mathcal{R} - \mathcal{I}_{4, L_1 L_2} \times_1 (\mathbf{A}_{\text{rx}} \boldsymbol{\Psi}) \times_2 (\mathbf{A}_{\text{tx}}^* \boldsymbol{\Phi}) \times_3 \mathbf{P}_B \times_4 \mathbf{F} \right\|_{\text{F}}, \quad (16)$$

which can be performed by means of the well-known alternating least squares (ALS) algorithm (see [16], [17] for details), which delivers estimates of the involved steering matrices up to scaling ambiguities provided that the necessary conditions $QNI \geq L_1 L_2$, $QMI \geq L_1 L_2$, and $QMN \geq L_1 L_2$ are satisfied [15]. These conditions are related to the uniqueness of the LS estimates of \mathbf{A}_{tx}^* , \mathbf{P}_B , and \mathbf{F} , respectively. The scaling ambiguities can be easily removed since the steering matrices have a Vandermonde structure.

B. Khatri-Rao and Kronecker Factorizations

To obtain individual estimates of the steering matrices \mathbf{B}_{rx} and \mathbf{B}_{tx} , as well as the fading coefficients \mathbf{f}_{β_i} and α_i , Khatri-Rao factorization (KRF) and Kronecker factorization (KF) procedures are applied by solving the following problems

$$\left\{ \hat{\mathbf{B}}_{\text{tx}}, \hat{\mathbf{B}}_{\text{rx}} \right\} = \arg \min_{\hat{\mathbf{B}}_{\text{tx}}, \hat{\mathbf{B}}_{\text{rx}}} \left\| \hat{\mathbf{P}}_B - \hat{\mathbf{B}}_{\text{rx}}^T \diamond \hat{\mathbf{B}}_{\text{tx}}^H \right\|_{\text{F}}^2, \quad (17)$$

$$\left\{ \hat{\beta}_i, \hat{\alpha}_i \right\} = \arg \min_{\beta_i, \alpha_i} \left\| \hat{\mathbf{f}}_i - \beta_i \otimes \alpha_i \right\|_2^2, i \in \{1, \dots, I\}, \quad (18)$$

the solutions of which are obtained by the KRF and KF algorithms as in [6] and [7], respectively. The estimated and

Algorithm 1 Stage 1 (PARKRON)

- 1: Transmit pilot signals with (1).
- 2: Estimate $\hat{\mathbf{u}}_i = \boldsymbol{\Omega}_i^\dagger \mathbf{y}_{i,1} \in \mathbb{C}^{MQN \times 1}$.
- 3: Build $\mathbf{R}_i = \text{unvec}_{MQ \times N}(\hat{\mathbf{u}}_i)$.
- 4: From $\{\mathbf{R}_1, \dots, \mathbf{R}_I\}$, build the tensor \mathcal{R} in (15).
- 5: Estimate $\hat{\mathbf{A}}_{\text{rx}}$, $\hat{\mathbf{P}}_B$, and $\hat{\mathbf{F}}$ by solving (16) using ALS.
- 6: Estimate $\hat{\mathbf{B}}_{\text{rx}}^T$ and $\hat{\mathbf{B}}_{\text{tx}}^H$ by solving (17) using KRF.
- 7: Estimate $\hat{\mathbf{F}}_\alpha$ and $\hat{\mathbf{F}}_\beta$ by solving (18) using KF.
- 8: Rebuild $\hat{\mathbf{R}}_1 = (\hat{\mathbf{A}}_{\text{tx}}^* \otimes \mathbf{A}_{\text{rx}}) \mathbf{D}_1(\hat{\mathbf{F}}) \hat{\mathbf{P}}_B^T$ and configure the IRS phase shifts from its dominant right singular vector.

Algorithm 2 Stage 2 (TBT)

- 1: Build the pilot tensor $\mathcal{Y}_i^{(p)}$ in (19)
- 2: Obtain an initial estimate $\hat{\mathbf{F}}_i$ according to (20).
- 3: Build the data tensor $\mathcal{Y}_i^{(d)}$ in (21).
- 4: Estimate $\hat{\mathbf{X}}_i^{(d)}$ and refine $\hat{\mathbf{F}}_i$ by solving (22) using BALS.

true matrices are linked as $\tilde{\mathbf{B}}_{\text{tx}} = \mathbf{B}_{\text{tx}} \Delta_{\mathbf{B}_{\text{tx}}}$, $\tilde{\mathbf{B}}_{\text{rx}} = \mathbf{B}_{\text{rx}} \Delta_{\mathbf{B}_{\text{rx}}}$, with $\Delta_{\mathbf{B}_{\text{tx}}} \Delta_{\mathbf{B}_{\text{rx}}} = \mathbf{I}_{L_1 L_2}$. Note that since these matrices have a Vandermonde structure, these scaling ambiguities can be removed by simple column normalization.

IRS phase-shift configuration: Upon estimation of the static channel parameters, IRS configuration is accomplished. Let $\hat{\mathbf{R}}_1 = (\hat{\mathbf{A}}_{\text{tx}}^* \otimes \mathbf{A}_{\text{rx}}) \mathbf{D}_1(\hat{\mathbf{F}}) (\hat{\mathbf{B}}_{\text{rx}}^T \diamond \hat{\mathbf{B}}_{\text{tx}}^H)^T$ be the reconstructed version of the combined channel in the first frame. The vector $\mathbf{s}_{\text{opt}} = [e^{j\theta_{1,\text{opt}}}, \dots, e^{j\theta_{N,\text{opt}}}]^T$ containing the configured IRS phase shifts can be found from the dominant right singular vector of $\mathbf{R}_1 = \mathbf{U}\boldsymbol{\Sigma}\mathbf{V}^H$, which gives $\mathbf{s}_{\text{opt}} = e^{-j\angle \mathbf{v}_1^*}$.

IV. CHANNEL TRACKING AND SYMBOL DETECTION

Under aging effects, the initial channel parameter estimates obtained in the first stage can quickly become outdated. This means that a further procedure is needed to track changes due to aging, if we intend to detect the transmitted symbols. To this end, we formulate the second stage of the proposed receiver, which is dedicated to channel tracking and symbol detection based on the estimated steering matrices in the first stage.

A. Initialization

From the pilot part of the received signal in (2), we have

$$\mathbf{Y}_{i,k}^{(p)} = \mathbf{A}_{\text{rx}} \mathbf{D}(\alpha_i) \mathbf{J} \mathbf{D}(\beta_{i,k}) \mathbf{C}_i^T + \mathbf{V}_{i,k}^{(p)} \in \mathbb{C}^{M \times T_p},$$

where $\mathbf{J} = \mathbf{B}_{\text{tx}}^H \mathbf{D}(\mathbf{s}_{\text{opt}}) \mathbf{B}_{\text{rx}}$, $\mathbf{C}_i^T = \mathbf{A}_{\text{tx}}^H \mathbf{X}_i^{(p)}$, and $\mathbf{V}_{i,k}^{(p)}$ is the associated AWGN component. Defining $\mathbf{y}_{i,k}^{(p)} = \text{vec}(\mathbf{Y}_{i,k}^{(p)})$ and using the equivalence $(\mathbf{a}^T \diamond \mathbf{B}) = \mathbf{B} \mathbf{D}(\mathbf{a})$ yields

$$\begin{aligned} \mathbf{y}_{i,k}^{(p)} &= (\mathbf{C}_i \otimes \mathbf{A}_{\text{rx}}) \text{vec}(\mathbf{D}(\alpha_i) \mathbf{J} \mathbf{D}(\beta_{i,k})) \in \mathbb{C}^{MT_p \times 1}, \\ &= (\mathbf{C}_i \otimes \mathbf{A}_{\text{rx}}) \mathbf{D}(\text{vec}(\mathbf{J})) (\beta_{i,k} \otimes \alpha_i) + \mathbf{v}_{i,k}^{(p)}. \end{aligned}$$

Then, defining $\mathbf{Y}_i^{(p)} = [\mathbf{y}_{i,1}^{(p)}, \dots, \mathbf{y}_{i,K}^{(p)}] \in \mathbb{C}^{MT_p \times K}$ collecting all remaining K blocks, we have

$$\mathbf{Y}_i^{(p)} = (\mathbf{C}_i \otimes \mathbf{A}_{\text{rx}}) \mathbf{D}(\text{vec}(\mathbf{J})) (\mathbf{F}_{\beta_i} \diamond \mathbf{F}_{\alpha_i})^T + \mathbf{V}_i^{(p)},$$

where $\mathbf{F}_{\alpha_i} = \mathbf{1}_K^T \otimes \alpha_i \in \mathbb{C}^{L_1 \times K}$, $\mathbf{F}_{\beta_i} = [\beta_{i,2}, \dots, \beta_{i,K+1}] \in \mathbb{C}^{L_2 \times K}$, and $\mathbf{V}_i^{(p)}$ is the corresponding noise term. Note that

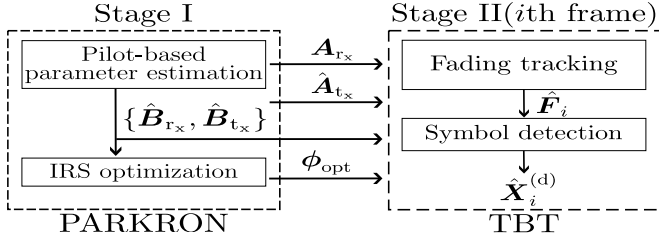


Fig. 2: Block-diagram of the proposed receiver.

$\mathbf{D}(\text{vec}(\mathbf{J})) \in \mathbb{C}^{L_1 L_2 \times L_1 L_2}$ can be viewed as the 3-mode unfolding of the tensor $\mathcal{J} \in \mathbb{C}^{L_1 \times L_2 \times L_1 L_2}$ written as [18]

$$\mathcal{J} = \left(\mathcal{I}_{3, L_2} \otimes_{2,3}^{2,3} \mathcal{I}_{3, L_1} \right) \times_3 \text{vec}(\mathbf{J}) \in \mathbb{C}^{L_1 \times L_2 \times L_1 L_2},$$

where \mathcal{I}_{3, L_2} and \mathcal{I}_{3, L_1} are identity tensors and $\otimes_{2,3}^{2,3}$ is the selective Kronecker product (SKP) [18], from which we obtain

$$\mathcal{Y}_i^{(p)} = \mathcal{J} \times_1 \mathbf{A}_{r_x} \times_2 \mathbf{C}_i \times_3 \mathbf{F}_i^T + \mathcal{V}_i^{(p)} \in \mathbb{C}^{M \times T_p \times K}, \quad (19)$$

where $\mathbf{F}_i = \mathbf{F}_{\beta_i} \diamond \mathbf{F}_{\alpha_i} \in \mathbb{C}^{L_1 L_2 \times K}$ is the combined fading matrix. The 3-mode unfolding of the tensor is defined as

$$[\mathcal{Y}_i^{(p)}]_{(3)} = \mathbf{F}_i^T [\mathcal{J}]_{(3)} (\mathbf{C}_i \otimes \mathbf{A}_{r_x})^T \in \mathbb{C}^{K \times M T_p},$$

from which an LS estimate of \mathbf{F}_i can be obtained as

$$\hat{\mathbf{F}}_i = \left[[\mathcal{Y}_i^{(p)}]_{(3)} \left([\hat{\mathcal{J}}]_{(3)} (\mathbf{C}_i \otimes \mathbf{A}_{r_x})^T \right)^\dagger \right]^T \in \mathbb{C}^{K \times L_1 L_2}. \quad (20)$$

This initial LS step requires that $[\mathcal{J}]_{(3)} (\mathbf{C}_i \otimes \mathbf{A}_{r_x})^T \in \mathbb{C}^{L_1 L_2 \times M T_p}$ have full row rank, which implies $M T_p \geq L P$.

B. Joint Tracking and Symbol Detection

From the data part of the received signal in (2), we have

$$\mathbf{Y}_{i,k}^{(d)} = \mathbf{A}_{r_x} \mathbf{D}(\alpha_i) \mathbf{J} \mathbf{D}(\beta_{i,k}) \mathbf{A}_{t_x}^H \mathbf{X}_i^{(d)} + \mathbf{V}_{i,k}^{(d)} \in \mathbb{C}^{M \times T_d},$$

which can be reformulated in tensor form as

$$\mathcal{Y}_i^{(d)} = \mathcal{J} \times_1 \mathbf{A}_{r_x} \times_2 (\mathbf{A}_{t_x}^H \mathbf{X}_i^{(d)})^T \times_3 \mathbf{F}_i^T + \mathcal{V}_i^{(d)} \in \mathbb{C}^{M \times T_d \times K} \quad (21)$$

The 2-mode and 3-mode unfoldings of $\mathcal{Y}_i^{(d)}$ are given by

$$\begin{aligned} [\mathcal{Y}_i^{(d)}]_{(2)} &= (\mathbf{A}_{t_x}^H \mathbf{X}_i^{(d)})^T [\mathcal{J}]_{(2)} (\mathbf{F}_i^T \otimes \mathbf{A}_{r_x})^T \in \mathbb{C}^{T_d \times M K}, \\ [\mathcal{Y}_i^{(d)}]_{(3)} &= \mathbf{F}_i^T [\mathcal{J}]_{(3)} \left[(\mathbf{A}_{t_x}^H \mathbf{X}_i^{(d)})^T \otimes \mathbf{A}_{r_x} \right]^T \in \mathbb{C}^{K \times T_d M}. \end{aligned}$$

Our joint tracking and symbol detection TBT algorithm consists of estimating the data matrix $\mathbf{X}_i^{(d)}$ while refining the estimate of \mathbf{F}_i initialized with (20) by solving

$$\left\{ \hat{\mathbf{X}}_i^{(d)}, \hat{\mathbf{F}}_i \right\} = \arg \min_{\mathbf{X}_i^{(d)}, \mathbf{F}_i} \left\| \mathcal{Y}_i^{(d)} - \mathcal{J} \times_1 \mathbf{A}_{r_x} \right\|_{\times_2 (\mathbf{A}_{t_x}^H \mathbf{X}_i^{(d)})^T \times_3 \mathbf{F}_i^T, \mathbb{F}}^2, \quad (22)$$

whose LS solutions are given by

$$\hat{\mathbf{X}}_i^{(d)} = \left[[\mathcal{Y}_i^{(d)}]_{(2)} \left(\mathbf{A}_{t_x}^* [\mathcal{J}]_{(2)} (\hat{\mathbf{F}}_i^T \otimes \mathbf{A}_{r_x})^T \right)^\dagger \right]^T, \quad (23)$$

$$\hat{\mathbf{F}}_i = \left[[\mathcal{Y}_i^{(d)}]_{(3)} \left([\mathcal{J}]_{(3)} \left((\mathbf{A}_{t_x}^H \mathbf{X}_i^{(d)})^T \otimes \mathbf{A}_{r_x} \right)^T \right)^\dagger \right]^T. \quad (24)$$

TABLE I: Computational complexity

Algorithm	Computational Complexity
PARKRON	$\mathcal{O}(L_1 L_2 (3 \text{ALS}_{\text{iter}} (L_1 L_2)^2 + N + I))$
TBT	$\mathcal{O}((L_1 L_2)^3 (1 + 2 \text{BALS}_{\text{iter}}))$
KRF	$\mathcal{O}(I K N L_1 L_2)$

The estimates of $\mathbf{X}^{(d)}$ and \mathbf{F}_i are obtained by alternating between the LS steps (23) and (24) using the bilinear alternating least squares (BALS) algorithm [6], which requires $M K \geq Q$ and $M T_d \geq L_1 L_2$. A summary of the channel tracking and symbol detection stage is shown in Algorithm 2.

Table I contains a summary of the computational complexities of the proposed PARKRON and TBT algorithms, as well as that of the competing KRF algorithm [6] used as a benchmark. The terms ALS_{iter} and $\text{BALS}_{\text{iter}}$ denote the number of iterations required for the convergence of the PARKRON and TBT algorithms, respectively. These results consider $\mathcal{O}(N_1 N_2)$ as the complexity associated with the rank-one approximation of a matrix $\mathbf{A} \in \mathbb{C}^{N_1 \times N_2}$. Since the KRF algorithm is a closed-form solution, it has lower computational complexity than the proposed receiver. However, note that KRF is limited to obtaining the unstructured estimates of \mathbf{G}_i and $\mathbf{H}_{i,k}$, i.e., it does not provide estimates of the channel parameters since the associated channel structures are not exploited. A block diagram of the overall receiver processing, including the first and second stages, is shown in Fig. 2.

V. SIMULATION RESULTS

We evaluate the performance of the proposed tensor-based algorithm by comparing it with the reference parameter estimation method based on the KRF [6]. The pilot signal matrix $\mathbf{X}^{(p)}$ is designed as a Hadamard matrix and the data signal matrix $\mathbf{X}^{(d)}$ follows a binary phase-shift keying (BPSK), while a discrete Fourier transform (DFT) is adopted for the IRS phase-shift matrix \mathbf{S} . The angular parameters $\phi_{\text{bs}}^{(l_1)}$ and $\phi_{\text{bs}}^{(l_2)}$ are randomly generated from a uniform distribution between $[-\pi, \pi]$ while the IRS elevation and azimuth angles of arrival and departure are randomly generated from a uniform distribution between $[-\pi/2, \pi/2]$. The fading coefficients α_i and $\beta_{i,k}$ are modeled as independent Gaussian random variables $\mathcal{CN}(0, 1)$. The parameter estimation accuracy is evaluated in terms of the NMSE given as $\text{NMSE}(\mathbf{Q}) = \mathbb{E} \left\{ \left\| \mathbf{Q}^{(e)} - \hat{\mathbf{Q}}^{(e)} \right\|_{\mathbb{F}}^2 / \left\| \mathbf{Q}^{(e)} \right\|_{\mathbb{F}}^2 \right\}$ with $\mathbf{Q} \in \{\mathbf{R}_i, \mathbf{W}_{i,k}\}$ being $\mathbf{R}_i = (\mathbf{H}_i^T \diamond \mathbf{G}_i)$ and $\mathbf{W}_{i,k} = \mathbf{G}_i \text{diag}(\mathbf{s}_{\text{opt}}) \mathbf{H}_{i,k}$ being used at the evaluation of the first stage and second stage at the e th run, $E = 10^4$ being the number of Monte Carlo runs. Symbol detection performance in the second stage is evaluated in terms of the bit error ratio (BER). Unless otherwise stated, the training SNR is set to 30 dB and the parameters are $\{M = 2, Q = 2, L_1 = 2, L_2 = 2, N = 32, T_0 = T = 64, T_p = 16, T_d = 48, I = 2, K = 5, \lambda = 0.75, \text{ and } \delta = 0.75\}$.

In Fig. 3, we compare the NMSE performance of the proposed technique at the first stage. We take the NMSE of \mathbf{R}_i after the PARAFAC ALS estimation and for comparison, we use the classical LS and KRF [6] estimators. We notice that the PARKRON and KRF algorithms both outperform the

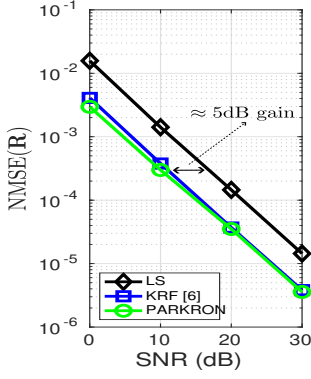


Fig. 3: NMSE at first stage.

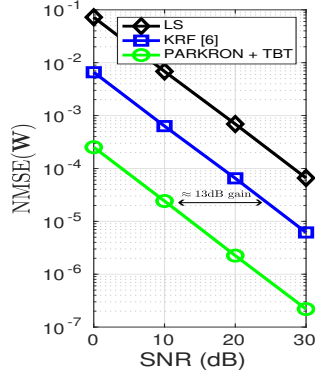


Fig. 4: NMSE at second stage.

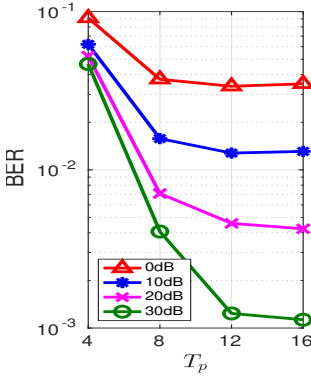


Fig. 5: BER as a function of number of pilot time-slots.

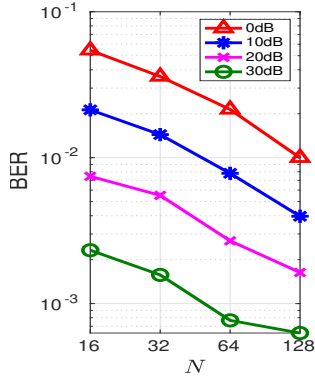


Fig. 6: BER as a function of the number of reflecting elements.

LS technique by approximately 5 dB, almost independently of the SNR. In Fig. 4, we take the NMSE of $\mathbf{W}_{i,k}$ after the TBT algorithm and compare our method with the KRF [6]. We note that, for different SNRs, the proposed PARKRON-TBT algorithm outperforms the KRF [6] with an approximate 13 dB gain. This could be explained by how the proposed technique exploits the channel geometry while the KRF [6] does not take advantage of the approximately fixed geometry of the transmission. However, KRF [6] is a closed-form solution having complexity $\mathcal{O}(IKNL_1L_2)$. In comparison, our proposed framework is an iterative solution with the complexity of $\mathcal{O}(L_1L_2(3\text{ALS}_{\text{iter}}(L_1L_2)^2 + N + I) + (L_1L_2)^3(1 + 2\text{BALS}_{\text{iter}}))$. Thus, our gains in NMSE come at the cost of greater computational complexity.

In Fig. 5, we study the effect of the number of pilot-reserved time slots, T_p , on the BER of the proposed algorithm. We observe that the BER improves as a function of the number of pilots as well as the SNR, as expected. Since the size of each block is set to $T = 64$ the saturation point of each curve is close to $T_p = 16$ (or 25% of the available time-slots). In Fig. 6, we evaluate the impact of the number N of reflecting elements. Since the number of reflecting elements is directly linked to the size of the blocks at the first stage, T_0 , as we increase N we have better estimations of the combined channel parameters in (12) since we sense the channel longer. For the proposed scenario, the performance gains of increasing N , only to achieve better BER performance, seems too low to justify the increased algorithm complexity.

VI. CONCLUSION

We proposed a two-stage framework for channel parameter estimation, tracking and symbol detection for MIMO IRS-assisted communications under a double-channel aging model. The proposed scheme estimates the static parameters in the first stage to initialize a second stage dedicated to data-aided tracking of the aging process to estimate the transmitted data symbols. The proposed PARKRON-TBT framework efficiently exploits the higher-order tensor structure of the considered channel aging model, providing improved performance over competing channel estimation schemes that do not exploit the double aging structure for tracking purposes at the cost of higher computational complexity.

REFERENCES

- [1] N. Rajatheva and *et al.*, "Scoring the terabit/s goal: Broadband connectivity in 6G," 2020, arXiv:2008.07220.
- [2] M. Di Renzo, A. Zappone, M. Debbah, M.-S. Alouini, C. Yuen, J. De Rosny, and S. Tretyakov, "Smart radio environments empowered by reconfigurable intelligent surfaces: How it works, state of research, and the road ahead," *IEEE J. Sel. Areas Commun.*, vol. 38, no. 11, pp. 2450–2525, 2020.
- [3] B. Zheng, C. You, W. Mei, and R. Zhang, "A survey on channel estimation and practical passive beamforming design for intelligent reflecting surface aided wireless communications," *IEEE Commun. Surv. Tutor.*, vol. 24, no. 2, pp. 1035–1071, 2022.
- [4] Q. Wu, S. Zhang, B. Zheng, C. You, and R. Zhang, "Intelligent reflecting surface-aided wireless communications: A tutorial," *IEEE Trans. Commun.*, vol. 69, no. 5, pp. 3313–3351, 2021.
- [5] S. Gong, X. Lu, D. T. Hoang, D. Niyato, L. Shu, D. I. Kim, and Y.-C. Liang, "Toward smart wireless communications via intelligent reflecting surfaces: A contemporary survey," *IEEE Commun. Surv. Tutor.*, vol. 22, no. 4, pp. 2283–2314, 2020.
- [6] G. T. de Araújo, A. L. de Almeida, and R. Boyer, "Channel estimation for intelligent reflecting surface assisted MIMO systems: A tensor modeling approach," *IEEE J. Sel. Top. Signal Process.*, vol. 15, no. 3, pp. 789–802, 2021.
- [7] G. T. de Araújo, P. R. Gomes, A. L. de Almeida, G. Fodor, and B. Makki, "Semi-blind joint channel and symbol estimation in IRS-assisted multi-user MIMO networks," *IEEE Wireless Commun. Lett.*, 2022.
- [8] C. Pan, G. Zhou, K. Zhi, S. Hong, T. Wu, Y. Pan, H. Ren, M. Di Renzo, A. L. Swindlehurst, R. Zhang *et al.*, "An overview of signal processing techniques for ris/irs-aided wireless systems," *IEEE J. Sel. Topics Signal Processing*, 2022.
- [9] G. Fodor, S. Fodor, and M. Telek, "Performance analysis of a linear MMSE receiver in time-variant Rayleigh fading channels," *IEEE Trans. Commun.*, vol. 69, no. 6, pp. 4098–4112, 2021.
- [10] B. Makki and T. Eriksson, "Feedback subsampling in temporally-correlated slowly-fading channels using quantized CSI," *IEEE Trans. Commun.*, vol. 61, no. 6, pp. 2282–2294, 2013.
- [11] Y. Cao, T. Lv, and W. Ni, "Two-timescale optimization for intelligent reflecting surface-assisted MIMO transmission in fast-changing channels," *IEEE Trans. Wireless Commun.*, 2022.
- [12] A. Papazafeiropoulos, I. Krikidis, and P. Kourtessis, "Impact of channel aging on reconfigurable intelligent surface aided massive MIMO systems with statistical CSI," *IEEE Trans. Veh. Technol.*, pp. 1–15, 2022.
- [13] R. W. Heath, N. Gonzalez-Prelcic, S. Rangan, W. Roh, and A. M. Sayeed, "An overview of signal processing techniques for millimeter wave MIMO systems," *IEEE J. Sel. Top. Signal Process.*, vol. 10, no. 3, pp. 436–453, 2016.
- [14] A. L. F. de Almeida, G. Favier, and J. C. M. Mota, "A constrained factor decomposition with application to MIMO antenna systems," *IEEE Trans. on Signal Processing*, vol. 56, no. 6, pp. 2429–2442, 2008.
- [15] A. Stegeman and A. L. F. de Almeida, "Uniqueness conditions for constrained three-way factor decompositions with linearly dependent loadings," *SIAM J. Matrix Anal. Appl.*, vol. 31, no. 3, pp. 1469–1490, 2010.
- [16] T. G. Kolda and B. W. Bader, "Tensor decompositions and applications," *SIAM review*, vol. 51, no. 3, pp. 455–500, 2009.
- [17] P. Comon, X. Luciani, and A. L. de Almeida, "Tensor decompositions, alternating least squares and other tales," *J. Chemom.*, vol. 23, no. 7–8, pp. 393–405, 2009.
- [18] B. Sokal, P. R. Gomes, A. L. F. de Almeida, and M. Haardt, "Tensor-based receiver for joint channel, data, and phase-noise estimation in MIMO-OFDM systems," *IEEE J. Sel. Top. Signal Process.*, vol. 15, no. 3, pp. 803–815, 2021.